JACS
JOURNAL OF THE AMERICAN CHEMICAL SOCIETY

Subscriber access provided by American Chemical Society

Article

Biosensing Using Porous Silicon Double-Layer Interferometers: Reflective Interferometric Fourier Transform Spectroscopy

Claudia Pacholski, Marta Sartor, Michael J. Sailor, Frdrique Cunin, and Gordon M. Miskelly

J. Am. Chem. Soc., **2005**, 127 (33), 11636-11645• DOI: 10.1021/ja0511671 • Publication Date (Web): 29 July 2005

Downloaded from http://pubs.acs.org on March 25, 2009

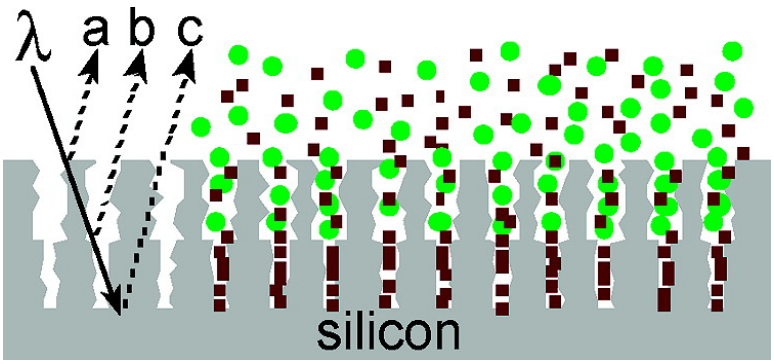

More About This Article

Additional resources and features associated with this article are available within the HTML version:

- Supporting Information
- Links to the 24 articles that cite this article, as of the time of this article download
- Access to high resolution figures
- Links to articles and content related to this article
- Copyright permission to reproduce figures and/or text from this article

View the Full Text HTML

ACS Publications
High quality. High impact.

Journal of the American Chemical Society is published by the American Chemical Society. 1155 Sixteenth Street N.W., Washington, DC 20036

J|A|C|S
ARTICLES
Published on Web 07/29/2005

Biosensing Using Porous Silicon Double-Layer Interferometers: Reflective Interferometric Fourier Transform Spectroscopy

Claudia Pacholski,[†] Marta Sartor,[†] Michael J. Sailor,*[,†] Frédérique Cunin,[‡] and Gordon M. Miskelly[§]

Contribution from the Department of Chemistry and Biochemistry, The University of California, San Diego, 9500 Gillman Drive, La Jolla, California 92093-0358, UMR CNRS/ENSCM 5618, 8 rue de l'école normale, 34296 Montpellier Cedex 5, France, and Department of Chemistry, The University of Auckland, Private Bag 92019, Auckland, New Zealand

Received February 23, 2005; E-mail: msailor@ucsd.edu

Abstract: A simple, chip-based implementation of a double-beam interferometer that can separate biomolecules based on size and that can compensate for changes in matrix composition is introduced. The interferometric biosensor uses a double-layer of porous Si comprised of a top layer with large pores and a bottom layer with smaller pores. The structure is shown to provide an on-chip reference channel analogous to a double-beam spectrometer, but where the reference and sample compartments are stacked one on top of the other. The reflectivity spectrum of this structure displays a complicated interference pattern whose individual components can be resolved by fitting of the reflectivity data to a simple interference model or by fast Fourier transform (FFT). Shifts of the FFT peaks indicate biomolecule penetration into the different layers. The small molecule, sucrose, penetrates into both porous Si layers, whereas the large protein, bovine serum albumin (BSA), only enters the large pores. BSA can be detected even in a large (100-fold by mass) excess of sucrose from the FFT spectrum. Detection can be accomplished either by computing the weighted difference in the frequencies of two peaks or by computing the ratio of the intensities of two peaks in the FFT spectrum.

1. Introduction

Porous Si is an attractive material for label-free chemical and biomolecule sensing due to its high surface area,[1] convenient surface chemistry,[2] and optical signal transduction capability.[3−9] Chemical or biomolecule detection can be based on changes in the spectral interference pattern that results from the reflection of white light at the interfaces above (air or solution) and below (crystalline Si) the porous Si layer. The spectral positions of the Fabry-Pérot fringes shift as a function of the refractive index of the material filling the pores.[10] Biomolecule penetration into the pores of porous Si layers, driven either by nonspecific adsorption[11−13] or by specific binding (to an antibody, for instance)[4,7] is observed as a shift of the Fabry-Pérot fringes to longer wavelengths. This corresponds to an increase in refractive index of the film as protein displaces aqueous solution in the pores.

To design an optical interferometric biosensor from porous Si, the pore size must be adjusted by appropriate choice of electrochemical etching conditions. The pores have to be large enough to allow the biomolecule of interest to enter but small enough to avoid light-scattering effects. These requirements can be met with the well-established methods for porous Si fabrication involving anodic dissolution of single-crystalline Si in HF-containing solutions. Depending on several parameters, such as Si wafer dopant type and resistivity, current density, and electrolyte composition, a wide range of pore sizes and morphologies can be obtained.[14,15] In addition, the pore diam-

[†] The University of California, San Diego.
[‡] UMR CNRS/ENSCM 5618.
[§] The University of Auckland.

(1) Hérino, R. In *Properties of Porous Silicon*; Canham, L., Ed.; Short Run Press Ltd.: London, 1997; Vol. 18, pp 89−96.
(2) Buriak, J. M. *Adv. Mater.* **1999**, *11*, 265−267.
(3) Lin, V. S.-Y.; Motesharei, K.; Dancil, K. S.; Sailor, M. J.; Ghadiri, M. R. *Science* **1997**, *278*, 840−843.
(4) Janshoff, A.; Dancil, K.-P. S.; Steinem, C.; Greiner, D. P.; Lin, V. S.-Y.; Gurtner, C.; Motesharei, K.; Sailor, M. J.; Ghadiri, M. R. *J. Am. Chem. Soc.* **1998**, *120*, 12108−12116.
(5) Zangooie, S.; Bjorklund, R.; Arwin, H. *Thin Solid Films* **1998**, *313−314*, 825−830.
(6) Snow, P. A.; Squire, E. K.; Russell, P. S. J.; Canham, L. T. *J. Appl. Phys.* **1999**, *86*, 1781−1784.
(7) Dancil, K.-P. S.; Greiner, D. P.; Sailor, M. J. *J. Am. Chem. Soc.* **1999**, *121*, 7925−7930.
(8) van Noort, D.; Welin-Klintstrom, S.; Arwin, H.; Zangooie, S.; Lundstrom, I.; Mandenius, C.-F. *Biosens. Bioelectron.* **1998**, *13*, 439−449.
(9) Chan, S.; Horner, S. R.; Miller, B. L.; Fauchet, P. M. *J. Am. Chem. Soc.* **2001**, *123*, 11797−11798.
(10) Gauglitz, G.; Brecht, A.; Kraus, G.; Nahm, W. *Sens. Actuators, B* **1993**, *11*, 21−27.
(11) Collins, B. E.; Dancil, K.-P.; Abbi, G.; Sailor, M. J. *Adv. Funct. Mater.* **2002**, *12*, 187−191.
(12) Karlsson, L. M.; Tengvall, P.; Lundström, I.; Arwin, H. *J. Colloid Interface Sci.* **2003**, *266*, 40−47.
(13) Karlsson, L. M.; Schubert, M.; Ashkenov, N.; Arwin, H. *Thin Solid Films* **2004**, *455−456*, 726−730.
(14) Zhang, X. G. *J. Electrochem. Soc.* **2004**, *151*, C69−C80.
(15) Foll, H.; Christopherson, M.; Carstensen, J.; Haase, G. *Mater. Sci. Eng., R* **2002**, *39*, 93−141.

10.1021/ja0511671 CCC: $30.25 **© 2005 American Chemical Society**

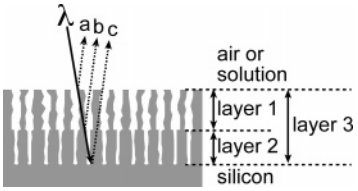

Figure 1. Schematic of the porous Si double-layer biosensor consisting of a top layer with large pores and a bottom layer with smaller pores. The three different interfering light beams are shown. Interference of beams a and b occurs from reflections at the interfaces bordering layer 1, interference of beams b and c originates from layer 2, and interference of beams a and c originates from layer 3. Analyte-containing solution is introduced at the top of the structure.

eters can be systematically varied in either horizontal or vertical directions (relative to the wafer surface), leading to pore gradient[11−13] and multilayer[16−18] structures.

Unlike the single-layered Fabry-Pérot films, biosensors based on porous Si multilayers have utilized optical transduction methods other than wavelength shifts of the interference pattern. For example, Martin-Palma et al. detected binding of polyclonal mouse antibodies to an amine-modified porous Si multilayer by observing a reduction in the intensity of reflected light.[19] Additionally, Chan et al. formed porous Si multilayer structures such as Bragg mirrors and microcavity resonators and used modulation of the photoluminescence spectra from these structures to distinguish between Gram(−) and Gram(+) bacteria.[9] The advantage of using a more elaborate optical structure is that the sensitivity of the measurement can be improved and the equipment needed to monitor binding events can be simplified. Incorporating more sophisticated functions such as correction for drifts due to thermal fluctuation, changes in sample composition, or degradation of the sensor matrix should also be possible with careful design of the optical structure.

A porous Si film containing a controlled distribution of pore sizes provides an example of a structure that performs a reasonably sophisticated function—in the present case discrimination of biomolecules by size. Porous Si films with a distribution of pore diameters in the $x-y$ plane (parallel to the surface of the wafer) have been demonstrated as size-exclusion matrices to perform an on-chip determination of macromolecule dimensions.[11] These films are generated by electrochemically etching Si in aqueous ethanolic HF using an asymmetric electrode configuration. Biomolecules penetrate the film and are detected only in regions where the pores are large enough. The disadvantage of this approach is that determination of protein size requires optical sampling over a relatively large area of the porous Si film.

This work describes a porous Si biosensor in which size discrimination occurs in the z direction (perpendicular to the plane of the wafer surface). The biosensor is composed of a porous Si layer with big pores on top of a layer with smaller pores (Figure 1). Light reflected from these porous Si double-layers contains three superimposed interference patterns (Figure 1), which can be resolved by fast Fourier transform (FFT) of the reflectivity spectrum. The three peaks in the FFT provide an indication of the relative partitioning of the large and small molecules in the two layers of this size-selective membrane. The concept is demonstrated using bovine serum albumin (BSA) and sucrose as the large and small probe molecules, respectively. Penetration of BSA exclusively into the top (large pore) layer and of sucrose into both layers is detected by the optical method, allowing the detection of the larger BSA in the presence of a 100-fold (by mass) excess of sucrose. The work here demonstrates a simple and powerful means to discriminate and detect molecules on the basis of size and to correct for drift in composition and other matrix effects with a designed nanostructure.

2. Results and Discussion

2.1. Fabrication and Stabilization of p-Type Porous Si Double-Layers. Porous Si double-layers with a layer of larger pores on top of a layer with smaller pores can be prepared using an electrochemical etch consisting of a short period of high applied current followed by a longer period at low current. In the present study, the current density profile consisted of 11 s at 500 mA/cm^2 followed by 55 s at 167 mA/cm^2. This waveform was applied to a highly doped (10^{-3} Ω-cm) p-type (100)-oriented single-crystal Si wafer in ethanolic HF solution. For comparison, the individual single-layer structures were also prepared. "Single-layer 1" was prepared using the first part of the double-layer waveform (11 s at 500 mA/cm^2), and "single-layer 2" was prepared using the second part of the double-layer waveform (55 s at 167 mA/cm^2). The resulting freshly etched porous Si samples are hydride-terminated and slowly degrade in air or water by oxidative or hydrolytic corrosion. To prevent corrosion in the aqueous solutions used in this study, siloxy-terminated porous Si surfaces were prepared by thermal oxidation.[20,21] Oxidation increases the hydrophilicity of porous Si, allowing water to effectively infiltrate the pores.

2.2. Determination of Porosity and Thickness of Porous Si Layers. The porosities and thicknesses of the individual porous Si layers were independently determined by gravimetry, SEM (thickness only) and by optical measurements. The average values obtained from at least three measurements are summarized in Table 1. Gravimetric measurements were performed by weighing the sample before etch, after etch, and after chemical dissolution of the porous layer, as previously described.[22] Cross-sectional scanning electron microscopy (SEM) reveals that the conditions used to prepare "single-layer 1" (11 s at 500 mA/cm^2) produce a ∼2600 nm-thick porous Si film with cylindrical pores possessing diameters of ∼50−100 nm (Figure 2A). The conditions used to prepare "single-layer 2" (55 s at 167 mA/cm^2) produce a film of ∼5400 nm in thickness (Figure 2B). The pores in this layer are smaller, with diameters that are too small to be reliably resolved in the SEM images (<20 nm). These results are in accordance with earlier work, in which an approximately exponential dependence of the pore diameter on the current density was found for highly doped p-type samples.[4] The porous Si double-layer, produced by

(16) Vincent, G. *Appl. Phys. Lett.* **1994**, *64*, 2367−2369.
(17) Berger, M. G.; Arens-Fischer, R.; Thoenissen, M.; Krueger, M.; Billat, S.; Lueth, H.; Hilbrich, S.; Theiss, W.; Grosse, P. *Thin Solid Films* **1997**, *297*, 237−240.
(18) Meade, S. O.; Yoon, M. S.; Ahn, K. H.; Sailor, M. J. *Adv. Mater.* **2004**, *16*, 1811−1814.
(19) Martín-Palma, R. J.; Torres-Costa, V.; Arroyo-Hernández, M.; Manso, M.; Pérez-Rigueiro, J.; Martínez-Duart, J. M. *Microelectron. J.* **2004**, *35*, 45−48.
(20) Lees, I. N.; Lin, H.; Canaria, C. A.; Gurtner, C.; Sailor, M. J.; Miskelly, G. M. *Langmuir* **2003**, *19*, 9812−9817.
(21) Gao, T.; Gao, J.; Sailor, M. J. *Langmuir* **2002**, *18*, 9953−9957.
(22) Halimaoui, A. In *Properties of Porous Silicon*; Canham, L., Ed.; Short Run Press Ltd.: London, 1997; Vol. 18, pp 12−22.

Table 1. Porosity and Thickness of Thermally Oxidized Porous Si Layers[a]

	gravimetry		spectral measurement[b]		SEM
porous Si Layer	porosity (%)	thickness (nm)	porosity (%)	thickness (nm)	thickness (nm)
single-layer 1	81 ± 1	2540 ± 40	85 ± 4	2890 ± 150	2570 ± 410
single-layer 2	64 ± 5	4440 ± 260	66 ± 4	5380 ± 160	5460 ± 210
double-layer:					
layer 1 (top)			88 ± 4	3010 ± 190	2940 ± 180
layer 2 (bottom)			63 ± 2	5310 ± 140	5640 ± 120
combination	71 ± 1[c]	7170 ± 450[c]	72 ± 2	8300 ± 300	8680 ± 120

[a] Porosities and thicknesses of porous Si single- and double-layers as determined by gravimetry, by spectral measurement, and by SEM. "Single-layer 1" was etched at 500 mA/cm^2 for 11 s, "single-layer 2" at 167 mA/cm^2 for 55 s, and "double-layer" at 500 mA/cm^2 for 11 s followed by 167 mA/cm^2 for 55 s. All samples have been thermally oxidized in air at 600 °C. [b] For the spectral measurement, calculation of porosity and thickness of "single-layer 1," "single-layer 2," and the top ("layer 1") and bottom ("layer 2") layers of "double-layer" is based on application of the Bruggeman approximation to the values of optical thickness (*nL*) obtained from FFT of the reflectivity spectra of samples immersed in various liquids, as described in the text. Porosity and thickness of "layer 1" in the porous silicon double layers is calculated using a value of EOT determined from the difference in EOT between "combination" (layer 3 in Figure 1) and "layer 2." [c] Gravimetric measurements do not distinguish between the two layers of the porous Si double-layers and provide an average value of porosity and thickness of both layers.

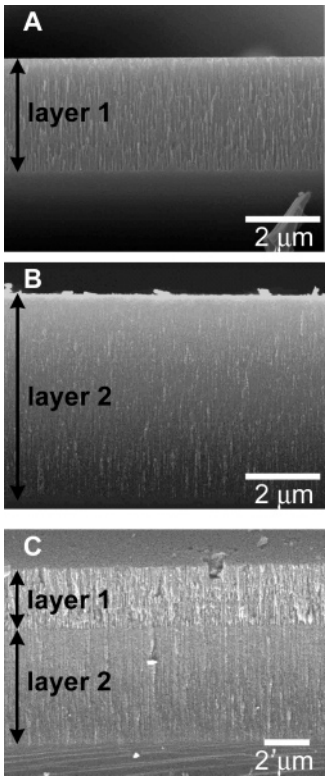

Figure 2. Cross-sectional scanning electron microscope (secondary electron) images of thermally oxidized porous Si single and double layers used in this study. (A) porous Si single-layer etched for 11 s at 500 mA/cm^2; (B) porous Si single-layer etched for 55 s at 167 mA/cm^2 and (C) porous Si double-layer etched for 11 s at 500 mA/cm^2 and then for 55 s at 167 mA/cm^2 to fabricate a large pore layer on top of a small pore layer. The electrolyte composition and the dopant concentration in the Si wafer are the same for all samples. Average values of layer thicknesses and porosities are given in Table 1.

applying the "single-layer 1" etching conditions followed immediately by the "single-layer 2" conditions, possesses a combination of the two single layers one on top of the other. The SEM image (Figure 2C) displays the macro/mesoporous structure, with layer thicknesses of ~2900 nm and ~5600 nm for layers 1 and 2, respectively.

Thickness and porosity of the layers were also determined by optical measurements. The Bruggeman theory,[23] one of a number of effective medium approximations,[24,25] has been shown to predict the porosity of porous Si in reasonable agreement with gravimetric determinations.[24,26] To obtain thickness and porosity values, the porous Si white-light reflection spectrum is measured with the film held in air and in the series of solvents ethanol, acetone, and hexane, having refractive indices 1.360, 1.357, and 1.375, respectively. The difference between the spectra can be attributed to the changes in optical thickness as the medium in the pores changes, with the assumption that all the void spaces in the film are filled equally (i.e., no remaining air bubbles). The values of the product 2*nL*, where *n* and *L* are the refractive index and the thickness of the film, respectively, are obtained from the reflectivity spectra as outlined in section 2.3, below. For the Bruggeman calculation, only the product *nL* is used. Data obtained from a given sample in air and in the three liquids are then fit to the two-component Bruggeman approximation,[27] yielding an over-determined solution for both the porosity and the thickness of the sample. The value of refractive index for oxidized porous Si that provided the most self-consistent results in the Bruggeman fit was 2.1. The calculated porosities of the porous Si single layers (Table 1) agree with the results obtained by gravimetry. However, the film thickness values obtained from the Bruggeman calculations and the SEM measurements deviate somewhat from the gravimetric results. The gravimetric measurements do not account for the increase in mass and in volume that occurs when the porous Si film is oxidized;[28] rather, gravimetry measures the amount of Si lost in etching. Thus, in the case of oxidized porous Si films, gravimetry provides an underestimation of film thickness. The SEM and optical measurements are more accurate measures of film thickness for the oxidized films used in this study.

2.3. Interpretation of Interferometric Reflectance Spectra. Figure 3 displays reflectivity spectra of thermally oxidized porous Si single- and double-layers. The spectra, obtained using a spectrometer and a white light (tungsten) illumination source in a 90° backscatter configuration, display a series of interference fringes. These fringe patterns result from Fabry-Pérot interference of light reflected from the various interfaces present in

(23) Bohren, C. F.; Huffman, D. R. *Adsorption and Scattering of Light by Small Particles*; Wiley: New York, 1983.
(24) Theiss, W.; Henkel, S.; Arntzen, M. *Thin Solid Films* **1995**, *255*, 177−180.
(25) Lee, C.; Koker, L.; Kolasinski, K. W. *Appl. Phys.* **2000**, 77−82.
(26) Anglin, E. J.; Schwartz, M. P.; Ng, V. P.; Perelman, L. A.; Sailor, M. J. *Langmuir* **2004**, *20*, 11264−11269.
(27) Zangooie, S.; Jansson, R.; Arwin, H. *J. Appl. Phys.* **1999**, *86*, 850−858.
(28) Astrova, E. V.; Voronkov, V. B.; Remenyuk, A. D.; Shuman, V. B.; Ioffe, A. F.; Tolmachev, V. A.; Vavilov, S. I. *Semiconductors* **1999**, *33*, 1149−1155.

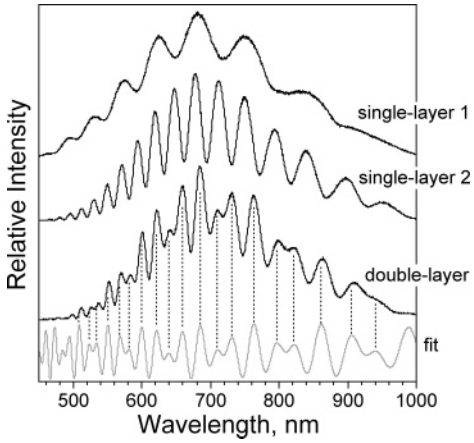

Figure 3. Relative reflectance spectra of thermally oxidized porous Si single- and double-layers. "single-layer 1" is the spectrum of a single layer represented by Figure 2A, etched for 11 s at 500 mA/cm^2, "single-layer 2" corresponds to the single layer shown in Figure 2B, etched for 55 s at 167 mA/cm^2, and "double-layer" corresponds to the double-layer sample shown in Figure 2C, etched for 11 s at 500 mA/cm^2, followed by 55 s at 167 mA/cm^2. "Fit" shows a least-squares fit of the double-layer spectrum to a two-layer interference model (eq 2) as described in the text. The peaks from the fit matching the spectral peaks are indicated with the vertical dashed lines. All spectra were obtained from a spot ~1 mm in diameter on the porous Si film. Spectra of samples were measured in air and are not corrected for instrumental spectral response.

Table 2. Comparison of Methods Used to Evaluate EOT (2*nL*) from the Reflectivity Spectrum: Fabry-Pérot Interference Calculation vs FFT[a]

porous Si Layer	fit to interference equations (nm)[b]	FFT(nm)
single-layer 1	7220	6950
single-layer 2	14,400	14,400
double-layer:		
layer 1 (top)	6200	6250
layer 2 (bottom)	13,800	13,900
combination	19,800	20,100

[a] Thermally oxidized porous Si layers as prepared in Table 1. [b] "Single-layer 1" and "single-layer 2" calculated from least-squares fit to eq 1. "Double-layer" calculated from least-squares fit to eq 2.

the structures.[10] The fringe maxima are described by the Fabry-Pérot relationship given in eq 1

$$m\lambda = 2nL \tag{1}$$

where m is an integer, L is the thickness of the porous Si layer, n is the average refractive index, and λ is the wavelength of incident light. The factor of 2 derives from the 90° backscatter configuration of the illumination source and detector. The term $2nL$ is thus the optical path, referred to as the effective optical thickness (EOT) in this work. The pore dimensions in these structures are too small to effectively scatter light, and each porous layer is treated as a single medium with a single refractive index value.

As expected from the relationship of eq 1, the series of Fabry-Pérot fringes observed in the "single-layer 1" and the "single-layer 2" samples are spaced evenly in frequency (Figure 3). A plot of m vs $1/\lambda_{max}$, where λ_{max} is the wavelength of each peak maximum and m is an integer, numbering each successive peak (increasing from long wavelength to short), yields a straight line, whose slope is equal to the quantity $2nL$ (Table 2). The double-layer film displays a more complex fringe pattern that cannot be fit to eq 1. The spectrum arises from interference in all three layers represented in Figure 1, and can be fit to a double layer interference model adapted from the treatment of McLeod.[29] Ignoring multiple reflections, the reflectance R of light from a double layer is given by:

$$R = (\rho_a^2 + \rho_b^2 + \rho_c^2) + 2\rho_a\rho_b\cos(2\delta_1) + 2\rho_b\rho_c\cos(2\delta_2) + 2\rho_a\rho_c\cos[2(\delta_1 + \delta_2)] \tag{2}$$

where δ_i represents the phase relationship of layer i:

$$\delta_i = \frac{2\pi n_i L_i}{\lambda} \tag{3}$$

Here n_i represents the refractive index of layer i with thickness L_i. The terms ρ_a, ρ_b, and ρ_c in eq 2 represent the index contrast at each of the interfaces a, b, or c (see Figure 1):

$$\rho_a = \frac{n_{air} - n_1}{n_{air} + n_1}, \quad \rho_b = \frac{n_1 - n_2}{n_1 + n_2}, \quad \rho_c = \frac{n_2 - n_{Si}}{n_2 + n_{Si}} \tag{4}$$

where n_{air}, n_1, n_2, and n_{Si} represent the refractive index of air (or of the solution), layer 1, layer 2, and bulk Si, respectively. The quantities n_1 and n_2 represent the total refractive index of the layer and everything it contains (silicon, SiO_2, solution, air, biomolecule, etc.). A least-squares fit of the reflectivity spectrum of the double layer to eq 2 is shown in Figure 3. The spectra shown in Figure 3 are not corrected for the spectral response of the lamp or spectrometer, and the values ρ_a, ρ_b, and ρ_c cannot be accurately evaluated from such data. Thus, the absolute intensity of the spectrum is not fit by the model. However, the phase relationship δ_i can be reliably extracted, yielding values of $2nL$ for layer 1 and for layer 2 of 6200 nm and 13 800 nm, respectively (Table 2). These values somewhat underestimate the single-layer values determined from eq 1 discussed above. Although the models used to fit the data are quite simplified, they provide a consistent picture of the optical properties of these structures.

2.4. Fast Fourier Transform (FFT) of Reflectance Spectra. Although a model incorporating the frequency dispersion of refractive index, the effect of multiple reflections, and the instrumental response function would provide a more rigorous description of the optical properties of the porous Si films, a faster and more convenient method of extracting the optical parameters is based on a fast Fourier transform (FFT) of the spectrum. The FFT can provide more reliable data for complicated optical structures, in particular when the optical constants are changing due to analyte admission into the pores. For the sensing application it will be seen that the relative change in these optical constants is the important parameter.

The Fourier transforms of the optical interference spectra of Figure 3 are presented in Figure 4. The value of $2nL$ can be obtained directly as the position of the peak in the FFT.[26] Thus, the "single-layer 1" film in air displays a spectral interference pattern (Figure 3) whose FFT yields a peak at 6950 nm (Figure 4 and Table 2). As mentioned above, the position of this peak in the FFT is equal to the value $2nL$ from eq 1. Similarly, the "single-layer 2" film displays a spectral interference pattern whose FFT yields a peak at 14,400 nm. If more than one layer exists in the film, the FFT yields values of $2nL$ for the separate layers as distinct peaks. Thus, the interference spectrum for the

(29) McLeod, H. A. *Thin-film Optical Filters*; Adam Hilger, Ltd.: Bristol, 1986; p 49.

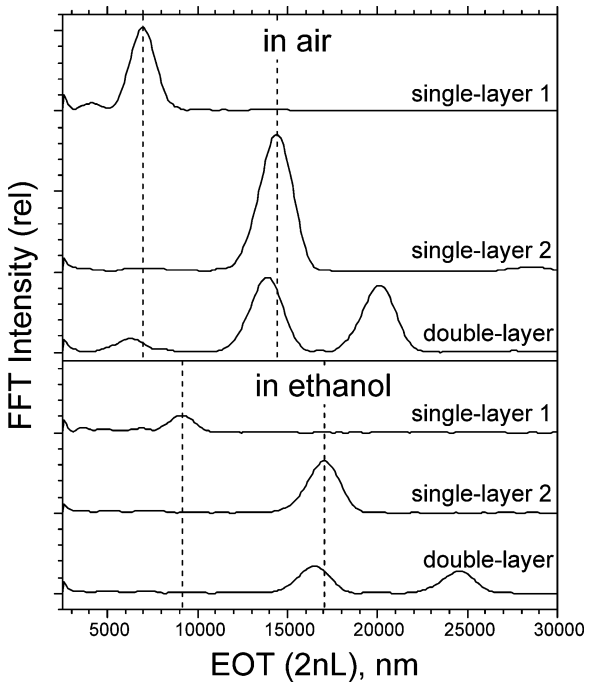

Figure 4. Fourier transforms of thermally oxidized p-type porous Si single- and double-layers in air and immersed in ethanol. "Single-layer 1" is the large pore layer, "Single-layer 2" is the small pore layer, and "double-layer" is the combination of both layers, prepared as in Figure 3. The corresponding reflectivity spectra for the "in air" samples are shown in Figure 3. The complex interference pattern for the double-layer is decomposed into its three components (layer 1, layer 2, and layer 1 + layer 2) by the Fourier transform. Peaks in the "in ethanol" spectra all display lower intensity relative to the corresponding "in air" spectra due to the decrease in refractive index contrast that occurs when the pores fill with liquid. All spectra were obtained from a spot ~ 1 mm in diameter, and are offset along the *y*-axis for clarity.

double-layer (Figure 3, "double-layer") has an FFT that displays three peaks (Figure 4, "double-layer") at 6250, 13 900, and 20 100 nm, corresponding to the values of 2*nL* for layers 1, 2, and 3, respectively, as depicted in Figure 1. Note that the sum of the values of 2*nL* for layer 1 and 2 is predicted by eq 2 to be equal to the value of 2*nL* for layer 3, and there is agreement within the error of the measurement (20 150 nm vs 20 100 nm, respectively). As with the least-squares fits of the spectra to eqs 1 and 2, the FFT analysis yields a 2*nL* value for each individual layer of the double-layer that is smaller than the value obtained from the corresponding single-layer, consistent with the SEM measurements (Table 1).

The information contained in both the intensity and in the position of the peaks in the Fourier transform can be related to the optical constants presented in the double-layer interference model of eq 2. As discussed above, the position of a peak in the FFT is equal to the EOT, or 2*nL* of a porous Si layer. It is related to the phase relationship of eq 3 by:

$$\mathrm{EOT}_i = 2n_iL_i = \frac{\lambda\delta_i}{\pi} \qquad (5)$$

Equation 2 represents a sum of three cosine terms corresponding to the three optical layers represented in Figure 1. The frequency of each of the cosine terms is thus related to the EOT of one of the layers. The amplitude of each cosine term is related to the amplitude of light reflected at the interfaces, and therefore related to the index contrast at each pair of interfaces that defines the relevant layer, as given by eq 4. The amplitude of a peak in the FFT spectrum is proportional to this index contrast:

$$A_1 = k\rho_a\rho_b, \quad A_2 = k\rho_b\rho_c, \quad A_3 = k\rho_a\rho_c \qquad (6)$$

where A_1, A_2, and A_3 are the amplitudes of the FFT peaks corresponding to layer 1, 2, and 3 of Figure 1, respectively, ρ_a, ρ_b, and ρ_c are as defined above for eq 4, and k is a proportionality constant. The relationship of FFT peak amplitude to index contrast is only strictly valid if the spectrum from which the FFT derives is an absolute reflectivity spectrum (corrected for instrument response). In that case, $k = 2$. In the present paper, uncorrected intensity-wavelength spectra are used. The FFT contains the necessary information to determine the optical constants of the films relevant for sensing, in particular, the refractive index of the film. The position of a given peak is a function of the refractive index of the layer, and the amplitude responds to the refractive index contrast of the layer, relative to its neighboring layers. The relationships of eqs 5 and 6 provide the key to extracting a reference channel from the double-layer interferometers described in this work.

2.5. Changes in the Optical Parameters Due to Infiltration of Ethanol. Infiltration of a liquid into the porous structures leads to predictable changes in both the position and in the intensity of the peaks in the FFT spectrum. The intensity changes correspond to changes in the relative reflectivity of the various interfaces in the structure. As seen in Figure 4, peaks in the FFT of spectra from the "in ethanol" samples all display lower intensity relative to the corresponding "in air" peaks. This is attributed to the decrease in refractive index contrast that occurs when the pores fill with liquid, as predicted by the relationships of eqs 4 and 6. Additionally, the peak corresponding to layer 1 of the double-layer, already weak in the "in air" spectrum, disappears completely in the "in ethanol" spectrum, indicating an almost complete disappearance of index contrast in that layer relative to the surrounding layers. The reduction in index contrast when a single-layer or double-layer film is immersed in liquid is also observed in the reflectivity spectrum, manifested as a decrease in fidelity of the Fabry-Pérot fringes.The decrease in intensity of the FFT peaks that occurs when the sample is immersed in liquid is most noticeable for samples that have been extensively oxidized, where the refractive index of the solid component of the porous film is closer to pure SiO_2 ($n = 1.5$) than to Si ($n = 3.8$). Ozone oxidation is milder, producing less SiO_2 in the film.[7] For a given porosity, ozone-oxidized films have a larger refractive index than thermally oxidized films, and the peak corresponding to layer 1 is more discernible in the FFT when such samples are immersed in liquids. However, the ozone-oxidized films were found to be insufficiently stable in the aqueous solutions and so were not used in the present study.

Shifts in the position of the peaks in the FFT spectrum indicate a change in average refractive index (EOT or 2*nL*) of the film. Infiltration of ethanol into the pores leads to an increase in the value of EOT for either the single- or the double-layer films. The "single-layer 1" film displays a spectrum with a peak in the Fourier transform at 6950 nm in air, increasing to 9080 nm in ethanol. Similarly, the FFT peak from the "single-layer 2" film shifts from 14 400 nm to 17 000 nm when the film is placed in the liquid.

The peaks in the FFT spectrum of the double-layer also shift upon infiltration of ethanol, in line with the single-layer results. As mentioned above, the peak corresponding to layer 1 of the double-layer structure often becomes too weak to observe upon immersion in ethanol due to the loss in index contrast, but the peaks corresponding to layer 2 and to the combination of both layer 1 and layer 2 ("layer 3" in Figure 1) are observable (Figure 4). Since the combination represents a sum of layers 1 and 2 (eq 2), the position of the peak corresponding to layer 1 can be calculated as the quantity ($EOT_3 - EOT_2$). Using this relationship, the $2nL$ value for layer 1 shifts by 1780 nm, from 6250 nm in air to 8030 nm in ethanol, and for layer 2 the shift is 2600 nm, from 13 900 nm to 16 500 nm.

2.6. Sensing of Bovine Serum Albumin and Sucrose in Double Layers. The penetration of biomolecules into a porous Si Fabry-Pérot layer leads to an increase in EOT resulting from partial replacement of aqueous buffer by molecules with a larger index of refraction. The magnitude of the increase in EOT for a given dose of analyte is dependent on three factors: (a) the size of the analyte, (b) the degree to which the analyte increases the refractive index of the buffer solution, and (c) the affinity of the porous Si surface for the analyte. Bovine serum albumin (BSA) and sucrose were used to test the ability of the porous Si double-layer to discriminate biomolecules of different sizes (factor a). BSA is a heart-shaped protein with dimensions roughly of the order of 3 nm × 8 nm × 8 nm (at pH 4) and a molecular mass of 68 kDa.[30] Sucrose is a small molecule with dimensions less than 2 nm × 2 nm × 2 nm, and a molecular mass of 342 Da. Because of the difference in pore dimensions between the two layers of the double-layer, both molecules are expected to be admitted into layer 1, and only sucrose is expected to enter into layer 2.

The second important factor in determining the change in EOT is the specific refractive index of the analyte (factor b). On an equal mass basis, most biomolecule solutions have similar refractive indices. In the case of the solutions used in the present study, the measured refractive index (Abbe refractometer, Bausch & Lomb, inc.) of a 1 mg/mL solution of BSA in pH 4 buffer is 1.3365, indistinguishable from that of pure buffer due to the relatively low concentration of protein. The measured refractive index of a 1 mg/mL solution of sucrose in pH 4 buffer is also 1.3365. Considering the error in the refractometer measurements of ±0.00005 and applying the Bruggeman model to a film with the porosity and thickness of layer 1 used in the present study, the interference relationship of eq 2 predicts a difference of less than ±0.5 nm in the value of EOT for these two solutions. A buffer solution containing 50 times more sucrose (50 mg/mL, $n = 1.3435$) is predicted to display an increase in EOT of 38 nm relative to pure buffer, well above the system detection limits. At the concentration used in the present paper, BSA should be undetectable unless it has an affinity for the surface that concentrates it in the oxidized porous Si film. This is the third factor that can contribute to an increase in EOT (factor c). As described below, the increase in EOT observed with BSA is much larger than expected due to significant nonspecific surface adsorption. In contrast, the increase observed with sucrose can be ascribed solely to its effect on the bulk refractive index of the solution in the pores.

Nonspecific adsorption of proteins to silica surfaces is an extremely complex process that depends on pH, temperature, ionic strength, and solvent properties.[31,32] The affinity of BSA for silica is well-established,[33] and for the silica surfaces used in the present study the BSA interaction is particularly strong. In previous work, attachment of poly(ethylene glycol)[34] or large biomolecules[7] to the inner pore surfaces has been used to minimize nonspecific adsorption to porous Si. In this work the surfactant Triton X-100 was added to the solutions to enhance diffusion of BSA out of the pores of thermally oxidized porous Si.[4] It was found that the initial introduction of BSA to the oxidized porous Si film always resulted in a small amount of very strongly bound BSA that was not removed with subsequent rinsing steps, even in the presence of surfactant or by changing pH. Sucrose did not display any such enhanced binding, and subsequent doses of either sucrose or BSA could be removed from the film. Presumably the oxidized porous Si surface contains a subset of reactive sites that bind strongly to BSA. To saturate these reactive sites, all samples used in the biomolecule sensing experiments were pretreated with a BSA solution and then rinsed with pH 7 buffer followed by pH 4 buffer prior to the introduction of analyte. After this "pretreatment" which led to a new baseline, both sucrose and BSA were found to diffuse readily into and out of the pores and to provide reproducible sensing curves during the flow cell experiments.

Even after the pretreatment described above, BSA displayed enhanced affinity (relative to sucrose) for the porous Si surface. However, this excess BSA could be removed by changing the pH of the solution. Aqueous buffer solutions of the test molecules were introduced to the porous Si films using a transparent flow-cell such that real-time reflectivity spectra could be obtained. The flow-cell was flushed with either pure pH 4 or pH 7 buffer followed by pure pH 4 buffer between samples. The purpose of the pH 7 rinse is to more efficiently remove the BSA molecule from the oxidized porous Si surface by changing the net charge on the molecule. The isoelectric point of BSA is 4.8; therefore, at pH 4 it has a net positive charge, while oxidized porous Si is negative, leading to strong nonspecific binding.[11,33] At pH 7 both BSA and oxidized porous Si are negatively charged, and electrostatic forces aid in expulsion of the protein from the pores.[11]

2.6.1. Shifts in FFT Peak Positions (EOT) on Exposure to BSA and Sucrose. The response of the layers can be probed using the FFT methods outlined above. As described in section 2.3, the interference spectrum of a double-layer film displays a complicated pattern of maxima and minima that corresponds to a combination of the Fabry-Pérot interference spectra from the three layers defined in Figure 1. The FFT decomposes the spectrum, and can distinguish between the filling of the big pores and the small pores. Figure 5 shows the shift of the two FFT peaks corresponding to layer 2 (the layer with small pores) and layer 3 (the combination of layers 1 and 2, see Figure 1) versus time during a flow cell experiment. For the experiment described by Figure 5, the sample was successively exposed to a buffer solution containing BSA with excess sucrose, sucrose alone, BSA alone, and then again BSA with sucrose.

(30) Huang, B. X.; Kim, H.-Y.; Dass, C. *J. Am. Soc. Mass. Spectrom.* **2004**, 1237−1247.
(31) Hlady, V.; Buijs, J. *Curr. Opin. Biotechnol.* **1996**, *7*, 72−77.
(32) Tarasevich, Y. I.; Monakhova, L. I. *Colloid J.* **2002**, *64*, 482−487.
(33) Su, T. J.; Lu, J. R.; Thomas, R. K.; Cui, Z. F. *J. Phys. Chem. B* **1999**, *103*, 3727−3736.
(34) Schwartz, M. P.; Cunin, F.; Cheung, R. W.; Sailor, M. J. *Phys. Status Solidi A* **2005**, *202*, 1380−1384.

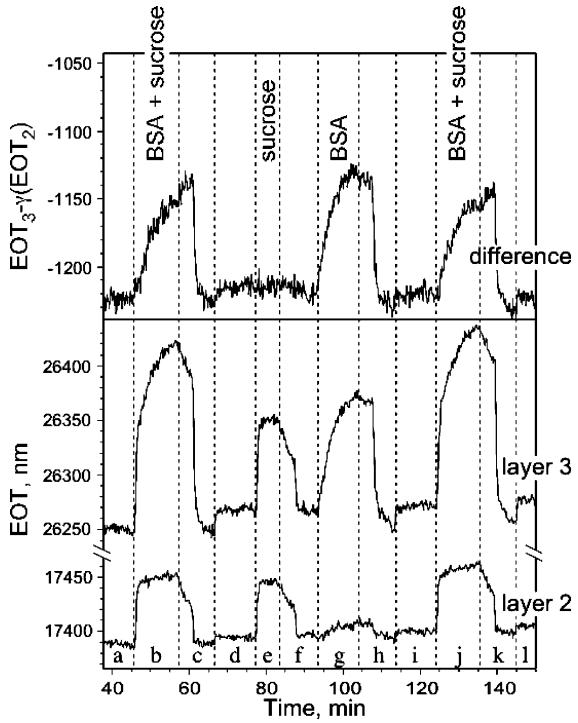

Figure 5. Effect of introduction of sucrose and bovine serum albumin (BSA), separately and in combination, on the effective optical thickness (EOT, or $2nL$) of layers 2 and 3 of a thermally oxidized double-layer sensor. EOT for a given layer is measured as the position of the corresponding peak in the FFT spectrum. Layer 2 contains the smaller pores, and does not respond to the larger BSA molecule. Layer 3 represents the combination of layer 1 and 2 (see Figure 1) and so responds to both BSA and sucrose. The weighted ($\gamma = 1.58$) difference of the EOT values from the two films, shown as the top trace, eliminates the effect of sucrose, allowing selective detection of BSA. (a) pH 4 buffer (potassium biphthalate); (b) 1 mg/mL BSA and 50 mg/mL sucrose in pH 4 buffer; (c) pH 4 buffer, followed by pH 7 buffer; (d) pH 4 buffer; (e) 50 mg/mL sucrose in pH 4 buffer; (f) pH 4 buffer; (g) 1 mg/mL BSA in pH 4 buffer; (h) pH 4 buffer, followed by pH 7 buffer; (i) pH 4 buffer; (j) 1 mg/mL BSA and 50 mg/mL sucrose in pH 4 buffer; (k) pH 4 buffer, followed by pH 7 buffer; (l) pH 4 buffer. All data were acquired under a constant peristaltic flow of 0.5 mL/min in a flow cell. Sample had been pretreated by exposure to BSA at pH 4 followed by a rinse with pure buffer at pH 7.

When the double-layer sample is exposed to a buffer solution containing 50 mg/mL of sucrose, the FFT peaks corresponding to layers 2 and 3 shift to larger values, corresponding to an increase in EOT as the solution infiltrates the pores (Figure 5, region **e**). The position of the peak assigned to layer 2 increases by ~50 nm, while the peak assigned to layer 3 shifts higher, by ~85 nm. The double-layer interference model of eq 2 predicts that the 50 mg/mL sucrose solution should increase the EOT of layer 2 by 52 ± 2 nm and of layer 3 by 90 ± 2 nm (using the measured value of the refractive index of the solution, the thickness and porosity values given in Table 1, and applying the Bruggeman effective medium approximation). Thus, the observed shifts agree with the mathematical model; sucrose solution is admitted into both regions of the film.

In contrast to sucrose, BSA only enters the layer with larger pores. When the double-layer sample is exposed to a buffer solution containing 1 mg/mL of BSA, the position of the peak assigned to layer 2 increases by <10 nm, and the peak assigned to layer 3 (the combination of layers 1 and 2) increases by ~100 nm (Figure 5, region **g**). As mentioned above, the double-layer interference model of eq 2 predicts that the 1 mg/mL BSA solution ($n = 1.3365$) should increase EOT of layer 1 (and thus layer 3) by less than 0.5 nm. The greater response that layer 3 displays toward BSA is ascribed to a nonspecific binding interaction of the protein in layer 1 as discussed above.[32] The data indicate that the concentration of BSA adsorbed to the surface of layer 1 is about 50-fold larger than the bulk solution concentration and that BSA does not enter layer 2 to any significant extent.

Data obtained with buffer solutions containing both BSA and sucrose (Figure 5, regions **b** and **j**) confirm the above conclusions that the small molecule, sucrose, can penetrate both layers 1 and 2 while the large protein, BSA, only enters layer 1. When the sample is exposed to solutions containing 1 mg/mL BSA and 50 mg/mL sucrose (Figure 5, regions **b** and **j**, respectively), the EOT value of layer 2 increases by approximately the same amount (~60 nm) as when only sucrose is added (~50 nm; Figure 5, region **e**). The EOT value of layer 3 increases by ~170 nm, close to the sum of the BSA-only (~100 nm; Figure 5, region **g**) and sucrose-only (~85 nm; Figure 5, region **e**) values. These data show that the response to this combination of analytes is additive.

2.6.2. Detection of Biomolecules in Double-Layers by Differential EOT Measurement. The main difference in composition between layers 1 and 2 is that layer 1 contains the protein BSA and layer 2, because of its smaller pores, does not. In addition, because they have different porosities, the relative amounts of SiO_2 and solution are different in each layer. If this latter difference can be accounted for, then a means to measure the incorporation of protein in the film results. Incorporation of protein can be measured as the difference in index between layer 1 (n_1) and layer 2 (n_2). Since the total refractive index of a layer is related to its EOT by eq 5, the difference can be expressed as:

$$\mathrm{EOT}_3 - \gamma\mathrm{EOT}_2 = n_1L_1 + n_2L_2(1 - \gamma), \qquad (7)$$

Here the term γ is a weighting factor that accounts for the differences in porosity and thickness between the two layers. It assumes that the index of a layer is proportional to its fractional composition, which is not strictly valid if the Bruggeman effective medium approximation applies. However, for small changes in n as encountered in the present biosensing application it is approximately correct. If $\gamma = 2$ and $L_1 = L_2$, the right side of eq 7 reduces to $(n_1 - n_2)L$, as expected. The quantity γ indicates how the relative responses of the two layers scale with each other, and can be determined empirically from the sucrose data by application of eq 8:

$$\gamma = \frac{\mathrm{EOT}_3(\text{sucrose}) - \mathrm{EOT}_3(\text{buffer})}{\mathrm{EOT}_2(\text{sucrose}) - \mathrm{EOT}_2(\text{buffer})} \qquad (8)$$

where EOT_i(sucrose) is the EOT measured for layer i infused with buffer containing sucrose, and EOT_i(buffer) is the EOT measured for layer i infused with buffer only. For the data in Figure 5, a value of 1.58 was determined for γ. A plot of the quantity $(\mathrm{EOT}_3 - \gamma\mathrm{EOT}_2)$ then detects BSA only, essentially nulling the response to sucrose (Figure 5).

2.6.3. Dependence of Differential EOT Measurement on Concentration of Matrix Interferents. The effect of a changing sample matrix on the differential EOT measurement is shown in Figure 6. In this experiment, a constant amount of BSA (1 mg/mL) is tested in the presence of sucrose concentrations

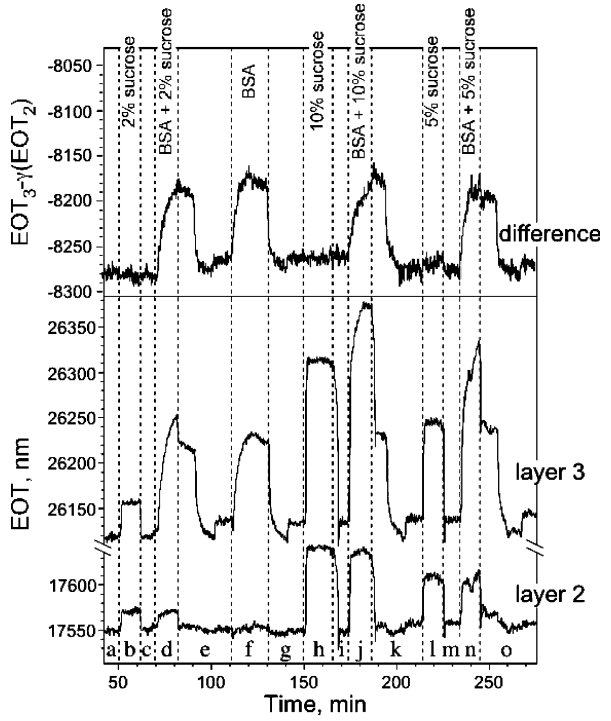

Figure 6. Dependence of the EOT values of a thermally oxidized double layer sensor toward BSA (1 mg/mL) in the presence of changing concentrations of sucrose. The weighted ($\gamma = 1.96$) difference of the EOT values from the two films, shown as the top trace, eliminates the effect of sucrose at all concentrations, allowing selective detection of BSA. The effective optical thickness (EOT, or 2*nL*) of layers 2 and 3 and the weighted difference of the two values are plotted as in Figure 5. Layer 2 contains the smaller pores and does not respond to the larger BSA molecule. Layer 3 represents layers 1 and 2 (see Figure 1) and so responds to both BSA and to sucrose. (a) pH 4 buffer; (b) 20 mg/mL sucrose in pH 4 buffer; (c) pH 4 buffer; (d) 1 mg/mL BSA and 20 mg/mL sucrose in pH 4 buffer; (e) pH 4 buffer, followed by pH 7 buffer, then by pH 4 buffer; (f) 1 mg/mL BSA in pH 4 buffer; (g) pH 4 buffer, followed by pH 7 buffer, then by pH 4 buffer; (h) 100 mg/mL sucrose in pH 4 buffer; (i) pH 4 buffer; (j) 1 mg/mL BSA and 100 mg/mL sucrose in pH 4 buffer; (k) pH 4 buffer, followed by pH 7 buffer, then pH 4 buffer; (l) 50 mg/mL sucrose in pH 4 buffer; (m) pH 4 buffer; (n) 1 mg/mL BSA and 50 mg/mL sucrose in pH 4 buffer; (o) pH 4 buffer, followed by pH 7 buffer, then pH 4 buffer. All data were acquired under a constant peristaltic flow of 0.5 mL/min in a flow cell. Sample had been pretreated by exposure to BSA at pH 4 followed by a rinse with pure buffer at pH 7.

varying from 0 to 100 mg/mL. The effective optical thickness (EOT, or 2*nL*) of layers 2 and 3 and the weighted difference of the two values are plotted as in Figure 5. As with the sample of Figure 5, the pores in layer 2 are too small to admit BSA, and this layer only responds to sucrose. Layer 3, consisting of both the large pore (layer 1) film and the small pore (layer 2) film, responds to both BSA and to sucrose. The weighted difference of the EOT values from the two films, shown as the top trace in Figure 6, completely eliminates the response from sucrose at all concentrations, allowing selective detection of BSA. For this sample the value of γ was determined to be 1.96 (by application of eq 8).

2.6.4. Detection of Biomolecules in Double-Layers by Measuring Shifts in FFT Peak Intensity. The amplitude of a peak A_i in the FFT spectrum is related to the reflectivity of the two interfaces bordering layer i by eq 6. The reflectivity at a given interface is related to the index contrast by eq 4. When protein infuses into either layer 1 or layer 2, it exerts an effect on the magnitude of A_i for both layers, since they share a common interface. Incorporation of protein can be measured

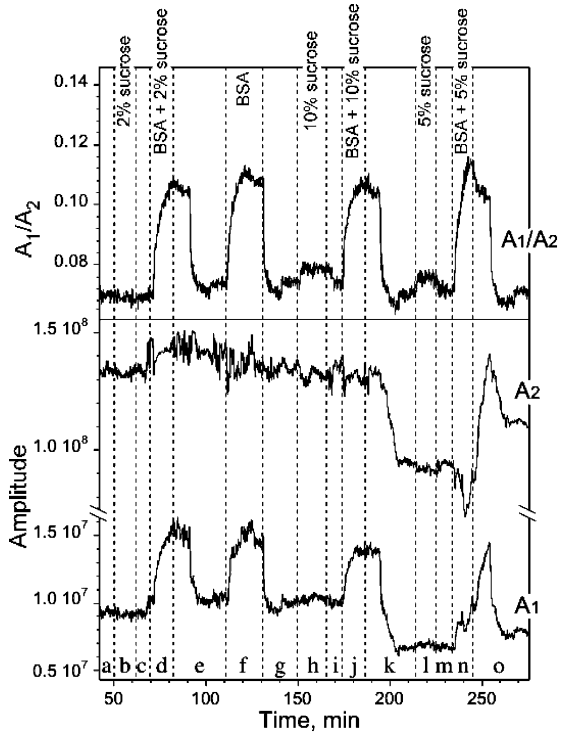

Figure 7. Dependence of the amplitude of the FFT peaks from the double layer sensor toward BSA (1 mg/mL) in the presence of changing concentrations of sucrose, as in Figure 6. A_1 and A_2 represent the integrated areas of the FFT peaks corresponding to layer 1 and layer 2 (A_1 and A_2 of eq 6), respectively. The ratio of A_1 to A_2 is shown in the top trace. The ratio eliminates the effect of sucrose at all concentrations, allowing selective detection of BSA. Note that the absolute scales for A_1 and A_2 differ. The labels (a−o) are the same as in Figure 6.

as the ratio of peak amplitudes A_1 to A_2. This ratio is related to the index contrast at two of the three interfaces present in the double-layer (eqs 4 and 6) by eq 9:

$$\frac{A_1}{A_2} = \frac{k\rho_a\rho_b}{k\rho_b\rho_c} = \frac{\rho_a}{\rho_c} \tag{9}$$

Here there is no weighting factor to account for differences in porosity and thickness between the two layers as was introduced in eq 7. In the present case the data deriving from layer 1 are used instead of those for layer 3. In some instances the amplitude A_1 in the FFT spectrum can be too small to measure reliably, especially when using fully oxidized porous Si (where the index contrast of layer 1 is small relative to those of its neighboring layers). In such cases it is also possible to isolate the response to BSA by plotting the ratio A_3/A_2.

The amplitude of the FFT peaks corresponding to layer 1 and layer 2 of the double-layer (A_1 and A_2), and the ratio of A_1 to A_2 are presented in Figure 7. The raw data sets from Figure 6 were used. As can be seen, the plots of A_1 and A_2 vs time are very noisy. The noise in the measurement relates to fluctuations in lamp intensity, bubbles in the flow cell, cell temperature, and other undetermined experimental variables during the course of the measurement. By contrast the measurement of EOT (FFT peak position) is much less sensitive to such variations. The errors apparent in the plots of A_1 and A_2 are correlated, and they are effectively eliminated in the ratio of A_1 to A_2, as shown in Figure 7. The quantity A_2 represents the product of the index contrast at both the bulk Si/layer 2 interface and the layer 1/layer

2 interface. It does not change significantly with either a large dose of sucrose or with BSA. The quantity A_1 represents the product of the index contrast at both the layer 1/layer 2 interface and the bulk solution/layer 1 interface, and it tracks the admission of protein into layer 1. Although A_2 appears to contain no information, it tracks lamp fluctuations, bubbles, and other sources of experimental error that also appear in A_1. In particular, note point *k* in the traces of Figure 7, the stage at which the largest dose of sucrose/BSA is removed; the relative reflectivity of the interfaces changes dramatically, but the ratio A_1/A_2 successfully nulls the effect.

3. Conclusions

This paper demonstrates a new means to construct an optical interferometer that incorporates a reference arm into the structure as a double-stack of porous layers, in a volume of less than 0.2 mm^3. This structure leads to optical fringes that provide information on processes occurring in each of the porous layers. It is shown how the important optical constants can be extracted by fast Fourier transform (FFT) of the reflectivity spectrum. The positions and amplitudes of the FFT peaks depend on the thicknesses and refractive indices of the layers. If one of these layers is appropriately designed, it can act as a blank (or reference) for the other layer. In the example we have used to demonstrate this concept, the pores in one of the layers have been made sufficiently small so as to exclude large biomolecules while smaller molecules (buffers and sugars) can penetrate both layers. When the structure is exposed to bovine serum albumin (BSA) at pH 4, the molecule can only access the outer (large pore) layer, and it adsorbs to the surfaces of those larger pores. This leads to changes in the refractive index of this layer only. When a mixture of BSA and smaller molecules is used, the smaller molecules again penetrate both layers, while the BSA only accesses the larger pore layer. The ratio of the amplitudes of the FFT peaks changes significantly when a molecule is present that can only enter the larger pores, allowing selective detection of this analyte. If the FFT peak positions, rather than their amplitudes are used, the changes in the selective (large-pore) layer can be corrected for effects of the presence of small molecules by linear subtraction of the appropriately weighted values. These methods provide a ready means for removing signals due to the presence of buffers and other small molecules such as sugars in a solution containing a large analyte.

Although the concept is demonstrated for separation and detection of biomolecules by size exclusion, the approach is generally applicable to chemical detection problems. For example, the methodology should also work if one layer contains a specific antibody. This would provide the device with an ability to discriminate on the basis of specific molecular affinity rather than nonspecific interaction. The methods exist to place molecules in specific layers of a porous Si multilayer,[35] and the use of antibodies or other specific capture probes in porous Si layers is well-established.[4,7,9,19,36,37] The approach should also be amenable to other label-free transduction modalities that utilize refractive index changes, such as surface plasmon resonance or microcavity resonance. The built-in reference channel and Fourier method of analysis provides a general means to compensate for changes in sample matrix, temperature, and other experimental fluctuations.

4. Experimental Section

Materials. All reagents were used as received. Potassium phosphate pH 7 buffer was obtained from Fisher, Inc. as a 0.05 M potassium phosphate Certified Buffer Solution (Cat. No. SB108-20). The potassium biphthalate pH 4 buffer was obtained from Fisher, Inc. as a 0.05 M potassium biphthalate Certified Buffer Solution (Cat. No. SB98-500). Bovine serum albumin (BSA), lyophilized powder, 1× crystallized, >97% purity, was obtained from Sigma-Aldrich (Cat. No. A 4378). Sucrose was obtained from EM Science (Cat. No. SX 1075-1). Aqueous HF (48%) and ethanol (99.9%) were supplied by Fisher Scientific and AAper, respectively. Porous Si samples were prepared from single-crystalline highly doped p-type Si (0.0008−0.0012 Ω-cm resistivity, ⟨100⟩ oriented, B-doped, from Siltronix Corp.)

Etching Procedure. Porous Si samples were prepared by anodization of the degenerately doped p-type Si wafers in ethanolic HF solution (3:1 v/v 48% aqueous HF:ethanol) in a two-electrode configuration using a platinum mesh counter-electrode. Si wafers with an exposed area of 1.2 cm^2 were contacted on the backside with a strip of aluminum foil and mounted in a Teflon etching cell. Galvanostatic anodization was performed in the dark. Single-layers were etched by applying 500 mA/cm^2 for 11 s ("single-layer 1") or 167 mA/cm^2 for 55 s ("single-layer 2"). Double-layer samples were prepared by application of 500 mA/cm^2 for 11 s followed immediately by application of 167 mA/cm^2 for 55 s. After etching, the samples were rinsed thoroughly with ethanol and then dried under a stream of nitrogen.

Scanning Electron Microscopy. Scanning electron microscopy (SEM) images were obtained with a Cambridge EM-360 electron microscope using an accelerating voltage of 20 keV. To avoid sample charging anomalies, the porous Si samples were sputter-coated with a thin layer of gold prior to the SEM analysis.

Interferometric Reflectance Spectra. Interferometric reflectance spectra of porous Si were collected by using an Ocean Optics CCD S-2000 spectrometer fitted with a microscope objective lens coupled to a bifurcated fiber optic cable. A tungsten light source was focused onto the center of a porous Si surface with a spot size of approximately 1−2 mm^2. Reflectivity data were recorded with a CCD detector in the wavelength range of 400−1000 nm, with a spectral acquisition time of 100 ms. Typically 10 spectral scans (1 s total integration time) were averaged before FFT processing. Both the illumination of the surface and the detection of the reflected light were performed along an axis coincident with the surface normal.

Thermal Oxidation. Porous Si samples were thermally oxidized by heat treatment in a tube furnace (Fisher Blue M). The samples were heated at 600 °C for 1 h in ambient air and then allowed to cool to room temperature.

Gravimetric Determination of Porosity and Thickness. Three porous Si samples were weighed on a laboratory balance with a resolution of 10 μg before (m_1) and after etching at mA/cm^2, respectively. Each sample was thermally oxidized and weighed again (m_2). The oxidized porous Si layer was then dissolved in 48% aqueous HF:ethanol (3:1, v:v), and the wafer remaining was weighed (m_3). The porosity P was calculated using the following equation:[22]

$$P = \frac{m_1 - m_2}{m_1 - m_3}$$

The thickness W of the porous Si layer was determined by applying the equation:

$$W = \frac{m_1 - m_3}{Sd}$$

(35) Link, J. R.; Sailor, M. J. *Proc. Nat. Acad. Sci. U.S.A.* **2003**, *100*, 10607−10610.
(36) Cunin, F.; Schmedake, T. A.; Link, J. R.; Li, Y. Y.; Koh, J.; Bhatia, S. N.; Sailor, M. J. *Nat. Mater.* **2002**, *1*, 39−41.
(37) Starodub, N. F.; Fedorenko, L. L.; Starodub, V. M.; Dikij, S. P.; Svechnikov, S. V. *Sens. Actuators, B* **1996**, *35*, 44−47.

where S is the wafer area exposed to HF during the electrochemical etching and d is the density of bulk Si.

Flow Cell Experiments. Biomolecule penetration experiments were carried out in a custom-made flow cell which has been described previously.[4] Briefly, the flow cell was constructed of plexiglass and connected via an outlet and inlet to a peristaltic pump. The light beam was focused on the surface of the sample through the Plexiglas cover and interference spectra were recorded.

Data Analysis. The wavelength axis of the spectrum from the Ocean Optics spectrometer was calibrated using a least-squares fit of five spectral lines observed from a neon lamp, at 585.3, 614.3, 640.2, 703.2, and 811.5 nm. The data spacing is approximately 0.4 nm. The x-axis was inverted and a linear interpolation was applied such that the data were spaced evenly in units of nm^{-1}. A Hanning window was applied to the spectrum, it was redimensioned to 4096 data points and zero padded to the power of two. A discrete Fourier transform using a multidimensional fast prime factor decomposition algorithm from the Wavemetrics, inc (www.wavemetrics.com) IGOR program library (FFT) was applied.

Acknowledgment. This project has been funded in part with Federal funds from the National Cancer Institute of the National Institutes of Health (Contract No. N01-C0-37117) and the Air Force Office of Scientific Research (Grant F49620-02-1-0288). C.P. thanks the Deutsche Forschungsgemeinschaft, (PA 925/1-1) for a postdoctoral fellowship. M.S. thanks the Fondazione Ing. Aldo Gini for a study grant. We thank Do-Kyung Kim for helpful discussions.

JA0511671